SIAM J. Applied Dynamical Systems
Vol. 15, No. 1, pp. 60–83

Phase Equation for Patterns of Orientation Selectivity in a Neural Field Model of Visual Cortex*

Samuel R. Carroll† and Paul C. Bressloff†

Abstract. In this paper we consider a neural field equation on $L\mathbb{R}^2 \times \mathbb{S}^1$, which models the activity of populations of spatially organized, orientation selective neurons. In particular, we show how spatially organized patterns of orientation tuning can emerge due to the presence of weak, long-range horizontal connections and how such patterns can be analyzed in terms of a reduced phase equation. The latter is formally identical to the phase equation obtained in the study of weakly coupled oscillators, except that now the spatially distributed phase represents the peak of an orientation tuning curve (stationary pulse or bump on S^1) of neural populations at different locations in $\mathbb{R}^2$. We then carry out a detailed analysis of the existence and stability of various solutions to the phase equation and show that the resulting spatially structured phase patterns are consistent with numerical simulations of the full neural field equations. In contrast to previous studies of neural field models of visual cortex, we work in the strongly nonlinear regime.

Key words. neural fields, phase equations, pattern formation, orientation tuning, visual cortex

AMS subject classification. 92C20

DOI. 10.1137/15M1016758

1. Introduction.

One of the striking characteristics of the early visual system is that the visual world is mapped onto the cortical surface in a topographic manner. This means that neighboring points in a visual image evoke activity in neighboring regions of primary visual cortex (V1). Superimposed upon the retinotopic map are additional maps reflecting the fact that neurons respond preferentially to stimuli with particular features [38]. Neurons in the retina, lateral geniculate nucleus, and primary visual cortex respond to light stimuli in restricted regions of the visual field called their classical receptive fields (RFs). Patterns of illumination outside the RF of a given neuron cannot generate a response directly, although they can significantly modulate responses to stimuli within the RF via long-range cortical interactions (see below). The RF is divided into distinct ON and OFF regions. In an ON (OFF) region illumination that is higher (lower) than the background light intensity enhances firing. The spatial arrangement of these regions determines the selectivity of the neuron to different stimuli. For example, one finds that the RFs of most V1 cells are elongated so that the cells respond preferentially to stimuli with certain preferred orientations. Similarly, the width of the ON and OFF regions within the RF determines the optimal spacing of alternating light and dark bars to elicit a response, that is, the cell's spatial frequency preference. Considerable information has been obtained about the spatial distribution of orientation selective cells in

*Received by the editors April 13, 2015; accepted for publication (in revised form) by J. Rubin December 3, 2015; published electronically January 20, 2016.
http://www.siam.org/journals/siads/15-1/M101675.html
†Department of Mathematics, University of Utah, Salt Lake City, UT 84112 (carroll@math.utah.edu, bressloff@math.utah.edu).

superficial layers 2/3 of V1 using a combination of microelectrode recordings [22] and optical imaging [6, 7, 5]. In particular, one finds that orientation preferences tend to rotate smoothly over the surface of cat and primate V1 (excluding orientation singularities or pinwheels), such that approximately every 300μm the same preference reappears. These experimental observations suggest that there is an underlying periodicity in the microstructure of V1. The fundamental domain of this approximate periodic (or quasi-periodic) tiling of the cortical plane is the so-called hypercolumn [27, 28, 29].

At least two distinct cortical circuits have been identified within superficial layers that correlate with the underlying feature preference maps. The first is a local circuit operating at submillimeter dimensions, in which cells make connections with most of their neighbors in a roughly isotropic fashion. It has been hypothesized that such circuitry provides a substrate for the recurrent amplification and sharpening of the tuned response of cells to local visual stimuli, as exemplified by the so-called ring model of orientation tuning [37, 4]. The other circuit operates between hypercolumns, connecting cells separated by several millimeters of cortical tissue, such that local populations of cells are reciprocally connected in a patchy fashion to other cell populations [32, 24]. Optical imaging combined with labeling techniques has generated considerable information concerning the pattern of these connections in superficial layers of V1 [30, 41, 8]. In particular, one finds that the patchy horizontal connections tend to link cells with similar feature preferences. Moreover, in certain animals such as tree shrew and cat there is a pronounced anisotropy in the distribution of patchy connections, with differing isoi-orientation patches preferentially connecting to neighboring patches in such a way as to form continuous contours following the topography of the retinotopic map [8]. There is also a clear anisotropy in the patchy connections of primates [36, 2]. However, in these cases most of the anisotropy can be accounted for by the fact that V1 is expanded in the direction orthogonal to ocular dominance columns [2]. Nevertheless, it is possible that when this expansion is factored out, there remains a weak anisotropy correlated with orientation selectivity. Moreover, patchy feedback connections from higher-order visual areas in primates are strongly anisotropic [2]. Stimulation of a hypercolumn via lateral connections modulates rather than initiates spiking activity [26], suggesting that the long-range interactions provide local cortical processes with contextual information about the global nature of stimuli. As a consequence horizontal and feedback connections have been invoked to explain a wide variety of context-dependent visual processing phenomena [23, 2].

One of the challenges in the mathematical and computational modeling of V1 cortical dynamics is developing recurrent networks models that incorporate details regarding the functional architecture of V1 [10]. This requires keeping track of neural activity with respect to both retinotopic and feature-based degrees of freedom such as orientation selectivity. (Analogous challenges hold for modeling other cortical areas.) In principle, one could construct a two-dimensional (20) neural field model of a superficial layer, in which neurons are simply labeled by retinocortical coordinates $\mathbf{r} = (x, y)$ in the plane $\mathbb{R}^2$. However, one then has to specify the nontrivial structure of the feature preference maps. An alternative approach was developed by Bressloff et al. [15, 14] within the context of geometric hallucinations, whereby the cortex is treated more abstractly as the product space $\mathbb{R}^2 \times \mathbb{S}^1$ with (coarse-grained) retinotopic coordinates $(x, y) \in \mathbb{R}^2$ and an independent orientation preference coordinate $\theta \in \mathbb{S}^1$, where $\mathbb{S}^1$ is the circle. The $\mathbb{R}^2 \times \mathbb{S}^1$ product structure of V1 superficial layers can be

incorporated into a continuum neural field model of the following form [15, 10]:

$$\tau\partial_t v(\mathbf{r},\theta,t) = -v(\mathbf{r},\theta,t) + \int_{\mathbb{R}^2}\int_{-\pi/2}^{\pi/2} w(\mathbf{r},\theta|\mathbf{r}',\theta')f(v(\mathbf{r}',\theta',t))d\theta' d\mathbf{r}' + I(\mathbf{r},\theta), \tag{1.1}$$

where $v(\mathbf{r},\theta,t)$ is the population activity at time t of neurons having orientation preference θ within the hypercolumn at retinotopic position $\mathbf{r}$. Here $w(\mathbf{r},\theta|\mathbf{r}',\theta')$ represents the synaptic weight distribution from neurons at $(\mathbf{r}',\theta')$ to neurons at $(\mathbf{r},\theta)$, $I(\mathbf{r},\theta)$ is an external input, and f is a sigmoidal rate function of the form

$$f(v) = \frac{1}{1+\mathrm{e}^{-\eta(v-\kappa)}}, \tag{1.2}$$

where η is the gain and κ is the threshold. We fix the units of time by setting $\tau = 1$ (typical physical values of τ are 1–10 ms). Following Bressloff et al. [15], the intracortical connections are decomposed into local connections within a hypercolumn and long-range patchy horizontal connections between hypercolumns:

$$w(\mathbf{r},\theta|\mathbf{r}',\theta') = w_{\mathrm{loc}}(\theta-\theta')\delta(\mathbf{r}-\mathbf{r}') + \varepsilon w_A(\mathbf{r}-\mathbf{r}',\theta)w_{\mathrm{hoz}}(\theta-\theta'), \tag{1.3a}$$

$$w_A(\mathbf{r},\theta) = w_s(\mathbf{r})A(\arg(\mathbf{r}-\mathbf{r}')-\theta) \tag{1.3b}$$

with w_{loc}, w_{hoz} and A even π-periodic functions of θ. We have introduced the small non-dimensional parameter ε, $0<\varepsilon\ll 1$, in order to reflect the fact that horizontal connections are weak and play a modulatory role. The local weight function w_{loc} is taken to be positive for small $|\theta|$ (neurons with similar orientation preferences excite each other) and negative for large $|\theta|$ (neurons with dissimilar orientation preferences inhibit each other). The θ-dependent part of the horizontal connections, w_{hoz}, is taken to be positive and narrowly peaked around zero so that only neurons with similar orientation preferences excite each other. The function A describes the anisotropy in the horizontal connections so that populations excite each other when the orientation preference at one location is in the same direction as the line connecting the two locations. The function $\arg(\mathbf{r})$ is the argument of the vector $\mathbf{r}$, or the angle between the vector and the x-axis. Finally, w_s, determines the strength of connections between two populations dependent only on the spatial separation of the populations. In this paper, we will assume that the horizontal connections are purely excitatory. However, our analysis applies to more general distributions.

Finally, we decompose the external input as

$$I(\mathbf{r},\theta) = I_0(\mathbf{r}) + \varepsilon I_1(\theta-\theta_0(\mathbf{r})),$$

where $I_1(\theta)$ is a symmetric function with peak at $\theta=0$ and $\theta_0(\mathbf{r})$ denotes the orientation of the input at location $\mathbf{r}$ and hence $I_1(\theta-\theta_0(\mathbf{r}))$ is peaked at the orientation of the stimulus. $I_0(\mathbf{r})$ represents background luminance or contrast at location $\mathbf{r}$. This particular form of the input reflects that the orientation component of the input to the network is weak and modulatory, whereas the orientation independent component is the main source of drive to cause the network to fire. Substituting the particular decomposition of w into (1.1) yields

$$\begin{aligned}\tau\partial_t v(\mathbf{r},\theta,t) = &-v(\mathbf{r},\theta,t) + w_{\mathrm{loc}}(\theta) * f(v(\mathbf{r},\theta,t)) + \varepsilon w_A(\mathbf{r},\theta)\circ w_{\mathrm{hoz}}(\theta) * f(v(\mathbf{r},\theta,t))\\ &+ I_0(\mathbf{r}) + \varepsilon I_1(\theta-\theta_0(\mathbf{r})),\end{aligned} \tag{1.4}$$

where

$$g(\mathbf{r}) \circ h(\mathbf{r},t) = \int_{\mathbb{R}^2} g(\mathbf{r}-\mathbf{r}')h(\mathbf{r}',t)d\mathbf{r}', \quad g(\theta) * h(\mathbf{r},\theta,t) = \int_{-\pi/2}^{\pi/2} g(\theta-\theta')h(\mathbf{r},\theta',t)d\theta'$$

and

$$g(\mathbf{r},\theta) \circ h(\theta) * f(\mathbf{r},\theta,t) = \int_{\mathbb{R}^2}\int_{-\pi/2}^{\pi/2} g(\mathbf{r}-\mathbf{r}',\theta)h(\theta-\theta')f(\mathbf{r}',\theta',t)d\theta' d\mathbf{r}'.$$

The $\mathbb{R}^2 \times \mathbb{S}^1$ neural field model (1.4), also known as a coupled ring model, has been used to study geometric visual hallucinations [15, 14], stimulus-driven contextual effects in visual processing [13, 35], and various geometric-based approaches to vision [31, 3, 34]. Extensions to incorporate other feature preference maps such as ocular dominance and spatial frequency [9] or variables associated with texture processing [17] have also been developed. Most of these studies assume that the neural field operates in a weakly nonlinear regime so that methods from bifurcation theory [20, 19, 10] can be used to analyze the formation of orientation selectivity patterns [15, 14, 13]. An alternative approach, which was originally introduced by Amari for 1D neural fields [1], is to assume that the neural field operates in a strongly nonlinear regime and to consider the high-gain limit of the sigmoidal rate function:

$$f(v) \to H(v-\kappa),$$

where $H(v)$ is the Heaviside function. In a recent paper, we used this method to study instabilities of stationary bumps and traveling fronts in a neural field with the product structure $\mathbb{R} \times \mathbb{S}^1$ [11]. In this paper we further develop the theory by analyzing solutions of the more realistic neural field model on $\mathbb{R}^2 \times \mathbb{S}^1$ given by (1.4). In particular we show how spatially organized patterns of orientation selectivity can emerge due to the presence of weak long-range horizontal connections and how such patterns can be analyzed in terms of a reduced phase equation. The latter is formally identical to the phase equation obtained in the study of weakly coupled oscillators [21, 39, 25], except that in our case the phase represents the peak of an orientation tuning curve. We begin in section 2 by considering stationary solutions of (1.4) in the absence of horizontal connections and orientation-dependent inputs ($\varepsilon = 0$). We identify parameter regimes whereby an orientation-independent input drives the spontaneous formation of orientation bumps, but the peaks of the bumps are highly uncorrelated in space. In section 3 we derive the phase equation that determines spatial correlations between the peaks of orientation bumps in the presence of weak, anisotropic horizontal connections. We then carry out a detailed analysis of the existence and stability of solutions to these phase equations in section 4 for particular choices of the weight functions and show in section 5 that the resulting spatially structured patterns of orientation selectivity are consistent with numerical simulations of the full neural field equations. Finally, in the discussion (section 6) we briefly discuss extensions to the case of orientation-dependent inputs.

2. Stationary solutions without horizontal connections. In the absence of horizontal connections and orientation-dependent inputs, $\varepsilon = 0$, (1.4) reduces to a system of uncoupled ring networks labeled by $\mathbf{r}$. For each $\mathbf{r}$ and a Heaviside rate function, stationary solutions satisfy the equation

$$V(\mathbf{r},\theta) = w_{\rm loc}(\theta) * H(V(\mathbf{r},\theta)-\kappa) + I_0(\mathbf{r}). \tag{2.1}$$

For simplicity we consider inputs to the network which are either on or off in certain regions. Therefore let $U \subset \mathbb{R}^2$ be the support of the input $I_0(\mathbf{r})$ and take $I_0(\mathbf{r}) = \gamma \mathbb{I}_U(\mathbf{r})$, where

$$\mathbb{I}_U(\mathbf{r}) = \begin{cases} 1, & \mathbf{r} \in U, \\ 0, & \mathbf{r} \notin U, \end{cases}$$

is the indicator function for the set U. It follows that

$$V(\mathbf{r},\theta) = V^+(\theta)\mathbb{I}_U(\mathbf{r}) + V^-(\theta)[1 - \mathbb{I}_U(\mathbf{r})] \tag{2.2}$$

with

$$V^-(\theta) = w_{\rm loc}(\theta) * H(V^-(\theta) - \kappa), \tag{2.3a}$$

$$V^+(\theta) = w_{\rm loc}(\theta) * H(V^+(\theta) - \kappa) + \gamma. \tag{2.3b}$$

We would like to consider a parameter regime where the presence of a localized input induces the formation of a stable orientation bump (stationary unimodal function of θ) in the region U, whereas the complementary region U^c remains quiescent due to the absence of an input. In order to determine an appropriate parameter regime, it is necessary to consider the Amari-based analysis of the ring model. We focus on (2.3b), since (2.3a) simply corresponds to the special case $\gamma = 0$.

Let us first consider θ-independent fixed point solutions of (2.3b). For the moment we drop the + superscript. If $\gamma < \kappa$, then the only fixed point is the subthreshold (down) state $V(\theta) = \bar{v}(\gamma) = \gamma$, whereas if $\kappa - w_0 < \gamma$, then the only fixed point is the superthreshold (up) state $V(\theta) = \bar{v}(\gamma) = w_0 + \gamma$, where

$$w_0 = \int_{-\pi/2}^{\pi/2} w_{\rm loc}(\theta) d\theta.$$

In both cases the fixed point is stable. Now consider a bump solution $V_0(\theta)$ that crosses a threshold at two points $\theta_\pm$, $V_0(\theta_\pm) = \kappa$. From translational and reflection symmetry around the ring, we can set $\theta_\pm = \pm\Delta$ so that $V_0(\Delta) = V_0(-\Delta) = \kappa$, where $\Delta < \pi/2$ is the bump half-width. It follows from substitution that

$$V_0(\theta) = W(\theta + \Delta) - W(\theta - \Delta) + \gamma \tag{2.4}$$

with

$$W(\theta) = \int_0^\theta w_{\rm loc}(\theta') d\theta'.$$

Imposing the threshold conditions then yields the following equation for Δ:

$$0 = -\kappa + W(2\Delta) + \gamma. \tag{2.5}$$

Suppose that $w_{\rm loc}$ has the property that there exists a unique $\theta^* \in (0, \pi/2)$ such that $w_{\rm loc}(\theta) \geq 0$ for $|\theta| \leq \theta^*$ and $w_{\rm loc}(\theta) < 0$ for $\theta^* < |\theta| \leq \pi/2$; see Figure 1(a). Such a weight function reflects short-range excitation and long-range inhibition. It is then clear that $W(\theta)$ has a

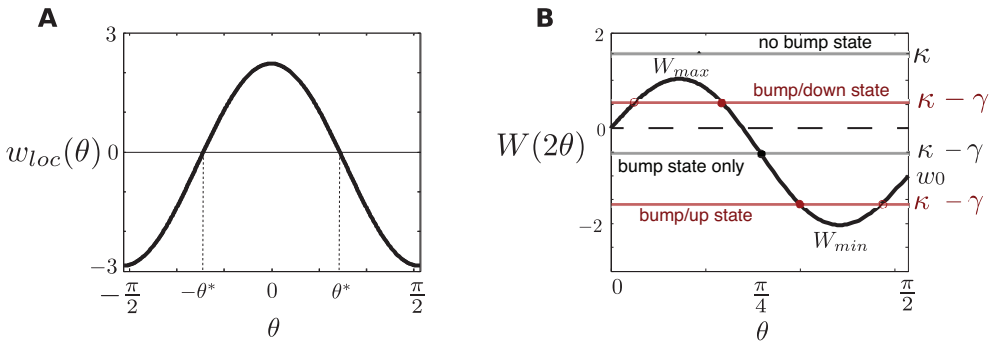

Figure 1. *Existence of bumps in the ring model. (a) Plot of Mexican hat local connections,* $w_{\rm loc} = (-1 + 8\cos(2\theta))/\pi$. *(b) Plot of* $W(2\theta)$. *The intercepts of* $W(2\theta)$ *with the horizontal line* $y = \kappa - \gamma$ *determine the bump solutions in the presence of a constant input* γ. *Stable solutions are indicated by a solid circle and unstable solutions by a hollow circle. In this parameter regime,* $\kappa > W_{max}$ *so that the zero state exists without a bump state and* $W_{min} < \kappa - \gamma < 0$ *so that the bump state coexists with the up state and without the zero state. Red indicates invalid parameter regime.*

unique local maximum, say, $W_{\rm max}$, at $\theta = \theta^*$ and a unique local minimum, say, $W_{\rm min}$, at $\theta = \pi - \theta^*$. This follows from the fact that $W'(\theta^*) = w_{\rm loc}(\theta^*) = 0 = w_{\rm loc}(\pi - \theta^*) = W'(\pi - \theta^*)$, and $W''(\theta^*) = w'_{\rm loc}(\theta^*) < 0$ while $W''(\pi - \theta^*) = w'_{\rm loc}(\pi - \theta^*) > 0$. Hence, a sufficient condition for the existence of a bump solution is $W_{\rm min} < \kappa - \gamma < W_{\rm max}$, which follows from the *intermediate value theorem*, which states that if a continuous function f with an interval $[a, b]$ as its domain takes values $f(a)$ and $f(b)$ at each end of the interval, then it also takes any value between $f(a)$ and $f(b)$ at some point within the interval. Although there may be more than one bump solution, there is only one stable solution (modulo translations) — the stability criterion is $W'(2\Delta) < 0$. Therefore the condition $W_{\rm min} < \kappa - \gamma < W_{\rm max}$ is necessary for stability. If we also impose the conditions $w_0 < 0$ and $\kappa < \gamma < \kappa + |w_0|$, then the bump does not coexist with an up or down state, i.e., there is no bistability. A graphical illustration of the various conditions is shown in Figure 1(b).

The location of the peak of the bump denotes the tuned orientation of a population in response to a stimulus. Therefore we require that a bump solution $V_0(\theta)$ has its maximum at $\theta = 0$ and therefore any translated bump $V(\theta - \theta_0)$ has its max at $\theta = \theta_0$. It is clear that a sufficient condition on $w_{\rm loc}$ is that it is an even function monotonically decreasing and one-to-one on the interval $[0, \pi/2]$. To see this, note that

$$V_0'(\theta) = w_{\rm loc}(\theta + \Delta) - w_{\rm loc}(\theta - \Delta).$$

Hence V is a max at θ_m only if

$$w_{\rm loc}(\theta_m + \Delta) = w_{\rm loc}(\theta_m - \Delta).$$

Furthermore, since $w_{\rm loc}$ is π-periodic this can be rewritten as

$$w_{\rm loc}(\theta_m + \Delta + n\pi) = w_{\rm loc}(\theta_m - \Delta), \quad n \in \mathbb{Z}.$$

But since $w_{\rm loc}$ is even and monotonic this occurs only when

$$\theta_m + \Delta + n\pi = -(\theta_m - \Delta) \implies \theta_m = \frac{n\pi}{2}.$$

Hence the extrema are located only at $\theta = 0, \pm\frac{\pi}{2}$ in the interval $[-\pi/2, \pi/2]$. By construction $V_0(0) > V_0(\pm\pi/2)$ and therefore the unique max is at $\theta = 0$. Furthermore it follows that the bump is monotonic when the weight function is monotonic, which is consistent with biologically realistic tuning curves.

Let us now apply these results to equations (2.3). We require that the only stable solution of (2.3a) is the zero solution $V^-(\theta) = 0$ and the only stable solution of (2.3b) is an orientation bump $V_0(\theta - \phi_0)$ with ϕ_0 arbitrary. The condition $\kappa > W_{\max}$ ensures that (2.3a) does not have a bump solution, whereas the condition $\kappa > \gamma = 0$ means that the zero solution exists and is stable. Therefore if $\kappa > W_{\max} > 0$, the zero state is the only fixed point to (2.3a). Turning to (2.3b), if $W_{\min} < \kappa - \gamma < 0 < \kappa - \gamma - w_0$ and $\kappa - \gamma < W_{\max}$, then there are no uniform steady state solutions, but there exists a unique stable bump solution. Note that $W_{\min} < 0$ is trivially satisfied by the assumption $w_0 < 0$. Hence, in this range the bump state is the only steady state solution to (2.3b). In conclusion, setting $V_-(\theta) = 0$ and $V_+(\theta) = V_0(\theta - \phi(\mathbf{r}))$ in (2.2) we obtain the solution

$$V(\mathbf{r}, \theta) = V_U(\mathbf{r}, \theta - \phi(\mathbf{r})) \equiv V_0(\theta - \phi(\mathbf{r}))\mathbb{I}_U(\mathbf{r}) \tag{2.6}$$

with $\phi(\mathbf{r})$ arbitrary. That is, in the active regions, neurons are tuned to an orientation at each corresponding position $\mathbf{r}$; however, the orientation structure is entirely uncorrelated. In the inactive regions, neurons are quiescent.

3. Horizontal connections and the phase equation. The incoherent structure for the phase of the bumps is an artifact of the lack of spatial structure in the local connections. We now show how weak long-range connections serve to correlate the bumps. We proceed by returning to the original system (1.4) with $0 < \varepsilon \ll 1$ and tracking the dynamics on two different timescales. Based on the fact that there is no time-varying phase when $\varepsilon = 0$, we expect that for $0 < \varepsilon \ll 1$ the phase will vary slowly. Furthermore we work in a parameter regime such that the bump solutions in the region U are stable and the zero state does not exist, while the zero state is stable outside of U and the bump state does not exist. Thus when we consider perturbed solutions for $\varepsilon > 0$ we are assured that there are no growth or decay of solutions due to instabilities inside U, as well as assured that the activity outside U remains below threshold. We therefore introduce the slow timescale $\tau = \varepsilon t$ and write the ansatz

$$v(\mathbf{r}, \theta, t, \tau) = V_U(\mathbf{r}, \theta - \phi(\mathbf{r}, \tau)) + \varepsilon v_1(\mathbf{r}, \theta - \phi(\mathbf{r}, \tau), t) + O(\varepsilon^2), \tag{3.1}$$

where the function v_1 serves as a corrective term in the perturbative expansion. Plugging this ansatz into (1.4) we obtain up to first order in ε (with $\tau = 1$)

$$\begin{aligned}
&\varepsilon\left[\partial_t v_1(\mathbf{r}, \theta - \phi(\mathbf{r}, \tau), t) - \partial_\tau \phi(\mathbf{r}, \tau)\partial_\theta V_U(\mathbf{r}, \theta - \phi(\mathbf{r}, \tau))\right] \\
&= -V_U(\mathbf{r}, \theta - \phi(\mathbf{r}, \tau)) + w_{\rm loc}(\theta) * H(V_U(\mathbf{r}, \theta - \phi(\mathbf{r}, \tau)) - \kappa) + \varepsilon\mathcal{L}_U v_1(\mathbf{r}, \theta - \phi(\mathbf{r}, \tau), t) \\
&\quad + \varepsilon w_A(\mathbf{r}, \theta) \circ w_{\rm hoz}(\theta) * H(V_U(\mathbf{r}, \theta - \phi(\mathbf{r}, \tau)) - \kappa) + \gamma\mathbb{I}_U(\mathbf{r}) + \varepsilon I_1(\theta - \theta_0(\mathbf{r})),
\end{aligned}$$

where

$$\mathcal{L}_U v(\mathbf{r}, \theta, t) = -v(\mathbf{r}, \theta, t) + \mathbb{I}_U(\mathbf{r}) w_{\rm loc}(\theta) * (H'(V_0(\theta) - \kappa)v(\mathbf{r}, \theta, t)). \tag{3.2}$$

(Note that since all Heaviside functions appear inside convolution integrals, we can formally carry out a perturbation analysis using distribution theory.) The $O(1)$ equation is given by (2.3) and is automatically satisfied by the bump solution V_0. After letting $\theta \to \theta + \phi(\mathbf{r},\tau)$, the $O(\varepsilon)$ equation takes the form

$$\partial_t v_1(\mathbf{r},\theta,t) - \mathcal{L}_U v_1(\mathbf{r},\theta,t) = \partial_\tau \phi(\mathbf{r},\tau) V_0'(\theta)\mathbb{I}_U(\mathbf{r}) + I_1(\theta+\phi(\mathbf{r},\tau)-\theta_0(\mathbf{r})) + \int_U w_A(\mathbf{r}-\mathbf{r}',\theta+\phi(\mathbf{r},\tau))V_{\rm hoz}(\theta+\phi(\mathbf{r},\tau)-\phi(\mathbf{r}',\tau))d\mathbf{r}',$$

where

$$V_{\rm hoz}(\theta) = W_{\rm hoz}(\theta+\Delta) - W_{\rm hoz}(\theta-\Delta), \quad W_{\rm hoz}(\theta) = \int_0^\theta w_{\rm hoz}(\theta')d\theta', \tag{3.3}$$

where Δ is the bump width for V_0. We can then consider the dynamics outside and inside U separately:

$$\partial_t v_1(\mathbf{r},\theta,t) + v_1(\mathbf{r},\theta,t) = I_1(\theta+\phi(\mathbf{r},\tau)-\theta_0(\mathbf{r})) + \int_U w_A(\mathbf{r}-\mathbf{r}',\theta+\phi(\mathbf{r},\tau))V_{\rm hoz}(\theta+\phi(\mathbf{r},\tau)-\phi(\mathbf{r}',\tau))d\mathbf{r}' \tag{3.4}$$

for $\mathbf{r} \notin U$ and

$$\partial_t v_1(\mathbf{r},\theta,t) - \mathcal{L}_\theta v_1(\mathbf{r},\theta,t) = \partial_\tau \phi(\mathbf{r},\tau) V_0'(\theta) + I_1(\theta+\phi(\mathbf{r},\tau)-\theta_0(\mathbf{r})) + \int_U w_A(\mathbf{r}-\mathbf{r}',\theta+\phi(\mathbf{r},\tau))V_{\rm hoz}(\theta+\phi(\mathbf{r},\tau)-\phi(\mathbf{r}',\tau))d\mathbf{r}' \tag{3.5}$$

for $\mathbf{r} \in U$, where

$$\mathcal{L}_\theta v(\mathbf{r},\theta,t) = -v(\mathbf{r},\theta,t) + w_{\rm loc}(\theta) * (H'(V_0(\theta)-\kappa)v(\mathbf{r},\theta,t)) \tag{3.6}$$

is the linear operator $\mathcal{L}_\theta$ acting on π-periodic functions of θ (for fixed $(\mathbf{r},t)$). We are primarily concerned with (3.5) since we wish to track the phase of the bumps only in the active regions. Note that the phase of the bump doesn't really make sense in the inactive region, since there are no bumps in this region. On the other hand (3.4) suggests that subthreshold activity is determined by the phase of the superthreshold activity. Furthermore, (3.5) is completely independent of (3.4) so that we can work solely with the former.

The linear operator $\mathcal{L}_\theta$ has a one-dimensional null space spanned by $V_0'(\theta)$ [10]. Let $\psi^\dagger(\theta)$ be an element of the null space of the adjoint operator $\mathcal{L}_\theta^\dagger$. Then it must satisfy

$$\mathcal{L}_\theta^\dagger \psi^\dagger \equiv -\psi^\dagger + H'(V_0(\theta)-\kappa)(w_{\rm loc}(\theta) * \psi^\dagger(\theta)) = 0, \tag{3.7}$$

where the adjoint is defined with respect to the inner product

$$\langle a, b\rangle = \int_{-\pi/2}^{\pi/2} a(\theta)b(\theta)d\theta.$$

We can then immediately see that if $\psi(\theta)$ is an element of the null space of $\mathcal{L}_\theta$, then

$$\psi^\dagger(\theta) = H'(V_0(\theta) - \kappa)\psi(\theta)$$

is an element of the null space of $\mathcal{L}_\theta^\dagger$. Thus the element of the adjoint null space is defined in the weak sense; that is, $\psi^\dagger$ is an adjoint null vector if

$$\langle \Psi, \mathcal{L}_\theta^\dagger \psi^\dagger(\theta)\rangle = 0$$

for all test functions $\Psi(\theta)$. Using the fact that

$$H'(V_0(\theta) - \kappa) = \frac{\delta(\theta - \Delta) + \delta(\theta + \Delta)}{|V_0'(\Delta)|},$$

we find that the distribution

$$\psi^\dagger(\theta) = [\delta(\theta - \Delta) + \delta(\theta + \Delta)]\, V_0'(\theta) \tag{3.8}$$

spans the null space of $\mathcal{L}^\dagger$. Existence of a bounded solution, v_1, to (3.5) requires that the right-hand side is orthogonal to all adjoint null vectors. Therefore, taking the inner product of (3.5) with $\psi^\dagger$ and setting it to zero by applying the Fredholm alternative theorem implies that the phase, $\phi(\mathbf{r}, \tau)$, has to satisfy the equation

$$\partial_\tau \phi(\mathbf{r},\tau) = -\frac{1}{\langle \psi^\dagger, V_0'\rangle}\Big[\int_U \langle \psi^\dagger, w_A(\mathbf{r}-\mathbf{r}', \theta + \phi(\mathbf{r},\tau) V_{\rm hoz}(\theta + \phi(\mathbf{r},\tau) - \phi(\mathbf{r}',\tau))\rangle d\mathbf{r}' \\ \langle \psi^\dagger, I_1(\theta + \phi(\mathbf{r},\tau) - \theta_0(\mathbf{r}))\rangle\Big].$$

Using (3.8) for the adjoint null vector, we have

$$\langle \psi^\dagger, V_0'\rangle = 2|V_0'(\Delta)|^2,$$
$$\langle \psi^\dagger, I_1\rangle = 2|V_0'(\Delta)|^2 I_O(\phi(\mathbf{r},\tau) - \theta_0(\mathbf{r})),$$

and

$$\langle \psi^\dagger, w_s(|\mathbf{r}-\mathbf{r}'|) A(\arg(\mathbf{r}'-\mathbf{r}) - \theta - \phi(\mathbf{r},\tau)) V_{\rm hoz}(\theta + \phi(\mathbf{r},\tau) - \phi(\mathbf{r}',\tau))\rangle \\ = 2|V_0'(\Delta)|^2 w_s(|\mathbf{r}-\mathbf{r}'|)\big[A_E(\arg(\mathbf{r}'-\mathbf{r}) - \phi(\mathbf{r},\tau)) P_O(\phi(\mathbf{r},\tau) - \phi(\mathbf{r}',\tau)) \\ - A_O(\arg(\mathbf{r}'-\mathbf{r}) - \phi(\mathbf{r},\tau)) P_E(\phi(\mathbf{r},\tau) - \phi(\mathbf{r}',\tau))\big],$$

where we have defined the functions

$$P_O(\theta) = V_{\rm hoz}(\theta - \Delta) - V_{\rm hoz}(\theta + \Delta), \qquad P_E(\theta) = V_{\rm hoz}(\theta - \Delta) + V_{\rm hoz}(\theta + \Delta),$$
$$A_E(\theta) = \frac{A(\theta + \Delta) + A(\theta - \Delta)}{4|V_0'(\Delta)|}, \qquad A_O(\theta) = \frac{A(\theta - \Delta) - A(\theta + \Delta)}{4|V_0'(\Delta)|},$$
$$I_O(\theta) = \frac{I_1(\theta - \Delta) - I_1(\theta + \Delta)}{2|V_0'(\Delta)|}.$$

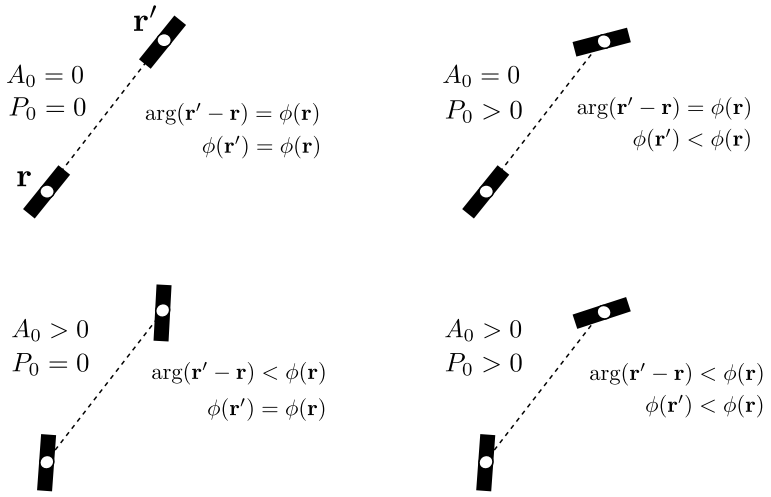

Figure 2. *Geometric interpretation of different forms of phase interactions in* (3.9). *See text for details.*

The final phase equation is thus given by

$$\begin{aligned}\partial_\tau \phi(\mathbf{r},\tau) = &- I_O(\phi(\mathbf{r},\tau) - \theta_0(\mathbf{r})) \\ &- \int_U w_s(|\mathbf{r}-\mathbf{r}'|)\big[A_E(\arg(\mathbf{r}'-\mathbf{r}) - \phi(\mathbf{r},\tau))P_O(\phi(\mathbf{r},\tau) - \phi(\mathbf{r}',\tau)) \\ &\qquad - A_O(\arg(\mathbf{r}'-\mathbf{r}) - \phi(\mathbf{r},\tau))P_E(\phi(\mathbf{r},\tau) - \phi(\mathbf{r}',\tau))\big]\end{aligned} \tag{3.9}$$

for all $\mathbf{r} \in U$.

The terms in the phase equation have an intuitive interpretation. Since I_O is a continuous odd function with $I_0'(0) \geq 0$, then when $\phi(\mathbf{r},\tau) \gtrless \theta_0(\mathbf{r})$ we have that $\partial_\tau\phi(\mathbf{r},\tau) \lessgtr 0$. Hence the phase moves toward the phase of the input, $\theta_0(\mathbf{r})$. When $\phi(\mathbf{r},\tau) = \phi(\mathbf{r}',\tau) = \arg(\mathbf{r}'-\mathbf{r})$, then $P_O = A_O = 0$, and the right-hand side of (3.9) is zero. When $\phi(\mathbf{r},\tau) \gtrless \phi(\mathbf{r}',\tau)$ and $\phi(\mathbf{r},\tau) = \arg(\mathbf{r}'-\mathbf{r})$, then $A_O = 0$ and $P_O \gtrless 0$. Thus $\partial_\tau\phi(\mathbf{r},\tau) \lessgtr 0$, so that the phase tends toward $\phi(\mathbf{r},\tau)$. When $\phi(\mathbf{r},\tau) = \phi(\mathbf{r}',\tau)$ and $\phi(\mathbf{r},\tau) \gtrless \arg(\mathbf{r}'-\mathbf{r})$, then $P_O = 0$ and $A_O \gtrless 0$. Thus $\partial_\tau\phi(\mathbf{r},\tau) \lessgtr 0$ and the phase moves toward $\arg(\mathbf{r}'-\mathbf{r})$. Hence, the first term, $A_E P_O$, represents responses to phase differences between two points when one of the phases has the same angle as the line connecting them. The second term, $A_O P_E$, represents responses to differences between the phase and the angle of the line when the phases at the two points are the same. The input term represents responses to differences between the solution and the phase of the stimulus. For a graphic illustration refer to Figure 2.

4. Analysis of the phase equation. We now analyze the existence and stability of some specific solutions to the phase equations in the case of no orientation-dependent inputs ($I_O = 0$). In section 5 we then compare our analytical results against numerical simulations of the full neural field equation and show good agreement between the two. Note that the existence of the phase solutions can be established under the quite general conditions on the weight kernels given in the introduction. We use only specific kernels in order to carry out the stability analysis.

4.1. Stationary solutions of the isotropic phase equation. Setting $A \equiv 1$ in (3.9) leads to the simplified phase equation

$$\partial_\tau \phi(\mathbf{r},\tau) = -\int_{\mathbb{R}^2} w_s(|\mathbf{r}-\mathbf{r}'|) P_O(\phi(\mathbf{r},\tau)-\phi(\mathbf{r}',\tau))d\mathbf{r}'. \tag{4.1}$$

Recall that $V_{\rm hoz}$ defined by (3.3) is an even π-periodic function and therefore P_O is an odd function with

$$P_O'(0) = 2\left(w_{\rm hoz}(0) - w_{\rm hoz}(2\Delta)\right) > 0.$$

Thus (4.1) is identical in form to the phase equation describing the phase of coupled neural oscillators considered in [21, 39, 25]. The only mathematical difference between the equations is that P_O is π-periodic, whereas the phase interaction function in coupled neural oscillators is taken to be 2π-periodic. This is merely due to the fact that rotation by π yields the same orientation, whereas the phase of oscillators takes any distinct value in $[0, 2\pi]$. A class of stationary solutions that have previously been studied within the context of weakly coupled phase oscillators is [21, 39, 25]

$$\phi_s(\mathbf{r}) = \mathbf{k}\cdot\mathbf{r} + \phi_0 \quad \forall \mathbf{k} \in \mathbb{R}^2, \quad \forall \phi_0 \in \mathbb{R}$$

with $\mathbf{k} = 0$ corresponding to the synchronous solution $\phi(\mathbf{r}) = \phi_0$. To see this we simply show that

$$\begin{aligned}\int_{\mathbb{R}^2} w_s(|\mathbf{r}-\mathbf{r}'|) P_O(\phi_s(\mathbf{r},\tau)-\phi_s(\mathbf{r}',\tau))d\mathbf{r}' &= \int_{\mathbb{R}^2} w_s(|\mathbf{r}-\mathbf{r}'|) P_O(\mathbf{k}\cdot(\mathbf{r}-\mathbf{r}'))d\mathbf{r}' \\ &= -\int_{\mathbb{R}^2} w_s(|\mathbf{r}'|) P_O(\mathbf{k}\cdot\mathbf{r}')d\mathbf{r}' = 0\end{aligned}$$

since w_s is even and P_O odd. Although the existence of stationary solutions of the form $\phi_s(\mathbf{r}) = \mathbf{k}\cdot\mathbf{r} + \phi_0$ is well-known, it turns out that the stability analysis of such solution has not been carried out fully in previous work. Therefore, it is useful to present the full analysis here.

Consider perturbations of the stationary solution given by

$$\phi(\mathbf{r},\tau) = \phi_s(\mathbf{r}) + \varepsilon\psi(\mathbf{r})e^{\lambda\tau} + O(\varepsilon^2).$$

Substituting this solution into (4.1) and Taylor expanding P_O to first order in ε yields the eigenvalue equation

$$\lambda\psi(\mathbf{r}) = -\int_{\mathbb{R}^2} w_s(|\mathbf{r}-\mathbf{r}'|) P_O'(\mathbf{k}\cdot(\mathbf{r}-\mathbf{r}'))(\psi(\mathbf{r})-\psi(\mathbf{r}'))d\mathbf{r}',$$

where we have neglected constants that don't contribute to stability. The eigenfunctions are of the form

$$\psi(\mathbf{r}) = e^{i\mathbf{q}\cdot\mathbf{r}}, \quad \mathbf{q} = q(\cos\theta_q, \sin\theta_q) \tag{4.2}$$

and the corresponding eigenvalues are given by

$$\lambda(\mathbf{q}) = -\int_{\mathbb{R}^2} w_s(|\mathbf{r}'|) P_O'(\mathbf{k}\cdot\mathbf{r}')\left(1 - e^{i\mathbf{q}\cdot\mathbf{r}'}\right)d\mathbf{r}' \tag{4.3}$$

Introducing the Fourier series

$$w_{\mathrm{hoz}}(\theta) = \frac{1}{\pi}\left[w_{\mathrm{hoz},0} + 2\sum_{n=1}^{\infty} w_{\mathrm{hoz,2n}} \cos(2n\theta)\right]$$

we find that

$$P'_O(\mathbf{k}\cdot\mathbf{r}') = \frac{16}{\pi}\sum_{n=1}^{\infty} \sin^2(n\Delta) w_{\mathrm{hoz,2n}} \cos(2n\mathbf{k}\cdot\mathbf{r}').$$

In order to evaluate the eigenvalue $\lambda(\mathbf{q})$ we recall some basic results in 2D Fourier transforms. Let $\mathcal{F}[w_s](\mathbf{q})$ denote the 2D Fourier transform of $w_s(\mathbf{r})$:

$$\mathcal{F}[w_s](\mathbf{q}) = \int_{\mathbb{R}^2} w_s(|\mathbf{r}'|) e^{i\mathbf{q}\cdot\mathbf{r}'} d\mathbf{r}' = \int_0^{\infty}\int_0^{2\pi} w_s(\rho) \mathrm{e}^{iq\rho\cos\theta} d\theta\, \rho d\rho.$$

Using the Jacobi–Anger expansion

$$e^{iz\cos\theta} = J_0(z) + 2\sum_{n=1}^{\infty} i^n J_n(z)\cos(n\theta), \tag{4.4}$$

where $J_n(z)$ is the nth order Bessel function of the first kind, yields

$$\mathcal{F}[w_s](\mathbf{q}) = 2\pi\int_0^{\infty} w_s(\rho) J_0(\rho q)\rho d\rho = 2\pi\mathcal{H}_0[w_s](q),$$

where $\mathcal{H}_n[w_s]$ is the nth order Hankel transform of w_s. It follows that

$$\lambda(\mathbf{q}) = \sum_{n=1}^{\infty} \sin^2(n\Delta) w_{\mathrm{hoz,2n}}[\mathcal{H}_0[w_s](|\mathbf{q}+2n\mathbf{k}|) + \mathcal{H}_0[w_s](|\mathbf{q}-2n\mathbf{k}|) - 2\mathcal{H}_0[w_s](2nk)], \tag{4.5}$$

where we have dropped a factor of 16. Convergence of the series follows from assuming that w_{hoz} has a convergent Fourier series. Note that

$$|\mathbf{q} \pm 2n\mathbf{k}|^2 = q^2 + 4n^2k^2 \pm 4nkq\cos(\theta_q - \theta_k),$$

and thus there is only a relative dependence on the direction of the solution, θ_k. The stability is then independent of the direction of $\mathbf{k}$ reflecting the rotational invariance of the system; however, it is still dependent on the magnitude k and the direction of perturbation, θ_q. Note that this is similar to the expression obtained in [25, 39]. However, [25] assumes that the 2D dynamics can be reduced to one dimension, which is not necessarily true, while [39] deals with dynamics on a ring. Therefore, in both cases they obtain an expression involving the Fourier transform of the corresponding 1D function w_s, rather than the Hankel transform of w_s of the full 2D model, which is simply the 2D Fourier transform of radially symmetric functions.

For the sake of illustration, consider the weight kernels

$$w_{\mathrm{hoz}}(\theta) = \frac{1}{\pi}\left[2 + 2\cos(2\theta)\right], \quad w_s(|\mathbf{r}|) = \frac{1}{2\pi\sigma^2} e^{-|\mathbf{r}|^2/2\sigma^2}. \tag{4.6}$$

i

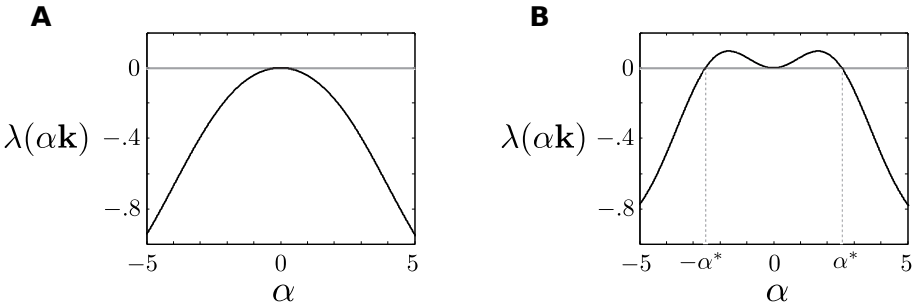

Figure 3. *Plot of eigenvalues for linear phase solution as given by (4.7b) with $\sigma = 0.5$ so that $k_c = 1$. (a) Eigenvalues for $k = 0.8$ ($k < k_c$). (b) Eigenvalues for $k = 1.2$ ($k > k_c$).*

The eigenvalues then become

$$\lambda(\mathbf{q}) = \sin^2(\Delta)\left[e^{-\sigma^2|\mathbf{q}+2\mathbf{k}|^2/2} + e^{-\sigma^2|\mathbf{q}-2\mathbf{k}|^2/2} - 2e^{-\sigma^2(2k)^2/2}\right].$$

It can be shown that eigenvalues assume their minimum and maximum values along the directions, $\mathbf{k}$ and $\mathbf{k}^\perp$. We therefore look at the eigenvalues at $\mathbf{q} = \alpha\mathbf{k}^\perp$ and $\mathbf{q} = \alpha\mathbf{k}$, neglecting the $\sin^2(\Delta)$ term,

$$\lambda(\alpha\mathbf{k}^\perp) = 2e^{-\sigma^2(2k)^2/2}\left(e^{-\sigma^2\alpha^2k^2/2} - 1\right), \tag{4.7a}$$

$$\lambda(\alpha\mathbf{k}) = e^{-\sigma^2(2k)^2(\alpha/2+1)^2/2} + e^{-\sigma^2(2k)^2(\alpha/2-1)^2/2} - 2e^{-\sigma^2(2k)^2/2}. \tag{4.7b}$$

Clearly $\lambda(\alpha\mathbf{k}^\perp) < 0$ for all $\alpha \neq 0$ and therefore the linear solution is always stable to perturbations in the orthogonal direction. The second case, $\mathbf{q} = \alpha\mathbf{k}$, is equivalent to reducing to one dimension and is analogous to the scenario in [25, 39]. As pointed out in [39], there are two qualitatively different behaviors for the eigenvalues for $k < k_c$ and $k > k_c$ where k_c is some critical value. If $k < k_c$, then $\lambda(\alpha\mathbf{k}) \leq 0$ with equality only at $\alpha = 0$ and is a monotonically decreasing function of α. For $k > k_c$, $\lambda(\alpha\mathbf{k}) \geq 0$ in the interval $[-\alpha^*, \alpha^*]$, with equality only at $\alpha = 0, \pm\alpha^*$, and $\lambda(\alpha\mathbf{k}) < 0$ on the interval $\mathbb{R} \setminus [-\alpha^*, \alpha^*]$. Hence, for intermediate values of α the eigenvalue is positive, whereas for large values of α the eigenvalue is negative. For the Gaussian it can be shown that $k_c^{-1} = 4\sigma$. Therefore if $k < 1/4\sigma$, then the linear phase solution is stable, whereas if $k > 1/4\sigma$, then it is unstable. The physical interpretation of this is if the wavelength $\nu = k^{-1}$ is greater than the range of the long-range connections then the solution is stable, while if it's less than the range it is unstable. For a graphical illustration of the eigenvalues in these two different regimes, see Figure 3.

4.2. Traveling wave solutions. To briefly consider an example of a phase equation with spatiotemporal dynamics, we introduce a shift asymmetry in the spatial part of the horizontal connections according to

$$w_s(|\mathbf{r} - \mathbf{r}'|) \to w_s(|\mathbf{r} - \mathbf{r}' - \mathbf{r}_0|).$$

Shift asymmetries in spatial connections have been used to study direction selectivity in neural populations responding to moving stimuli [40, 16]. We find that traveling phase waves of the

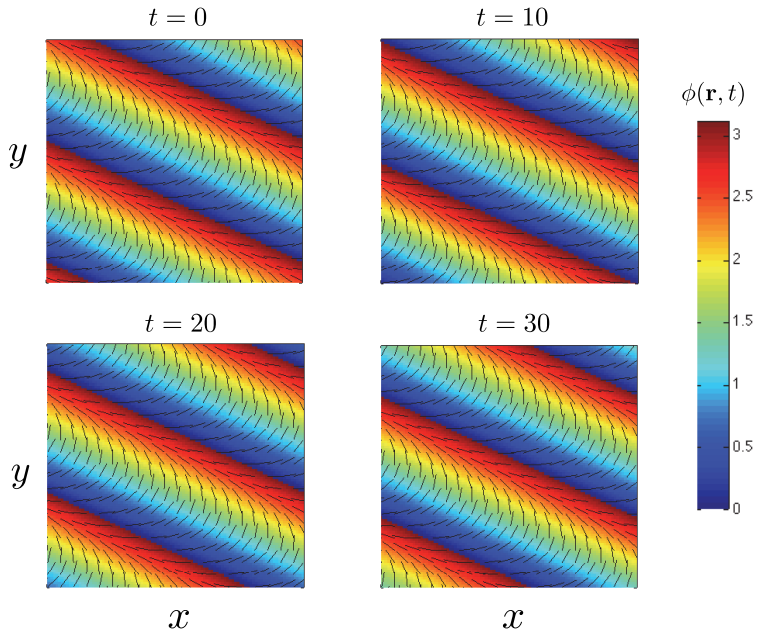

Figure 4. *Plot of numerical simulations of the full neural field equation (1.4) showing the propagation of a linear phase wave. In order to illustrate the variation in the peak of orientation bumps as a function of spatial position, we discretely sample a set of orientations and draw a short bar of a given orientation at the spatial locations where the corresponding peaks occur. We also use a color code to emphasize the regions of constant orientation. The wavevector* $\mathbf{k}$ *of the phase wave is orthogonal to these regions.*

form $\phi(\mathbf{r}, \tau) = \mathbf{k} \cdot \mathbf{r} - c\tau$ are solutions to (3.9) with $A \equiv 1$. That is,

$$c(\mathbf{r}_0) = -\int_{\mathbb{R}^2} w_s(|\mathbf{r} - \mathbf{r}' - \mathbf{r}_0|) P_O(\mathbf{k} \cdot (\mathbf{r} - \mathbf{r}')) d\mathbf{r}' = \int_{\mathbb{R}^2} w_s(|\mathbf{r}'|) P_O(\mathbf{k} \cdot (\mathbf{r}' - \mathbf{r}_0)) d\mathbf{r}',$$

and therefore the wavespeed, c, is determined explicitly by the integral on the right-hand side and is dependent on the shift, $\mathbf{r}_0$. Note that if $\mathbf{r}_0 = \mathbf{k}^\perp$, then

$$c(\mathbf{k}^\perp) = \int_{\mathbb{R}^2} w_s(|\mathbf{r}'|) P_O(\mathbf{k} \cdot (\mathbf{r}' - \mathbf{k}^\perp)) d\mathbf{r}' = \int_{\mathbb{R}^2} w_s(|\mathbf{r}'|) P_O(\mathbf{k} \cdot \mathbf{r}') d\mathbf{r}' = 0$$

and that $c(-\mathbf{r}_0) = -c(\mathbf{r}_0)$. Thus, if the shift $\mathbf{r}_0$ is in the direction along which the solution is constant for fixed τ, $\mathbf{r}_0 = \mathbf{k}^\perp$, then there is no wave propagation, and the solution reverses its direction of propagation under the transformation $\mathbf{r}_0 \to -\mathbf{r}_0$. It then appears that the direction of the asymmetry controls the direction of propagation. The existence of a phase solution in the full system can be confirmed by numerically solving the neural field equation (1.4). In Figure 4 we plot snapshots of the time evolution of such a solution which clearly illustrates the propagation of a linear phase wave as predicted by the phase equation.

4.3. Synchronous solution of the anisotropic phase equation. Stationary solutions to the anisotropic phase equation (3.9) satisfy the equation

$$0 = \int_{\mathbb{R}^2} w_s(|\mathbf{r} - \mathbf{r}'|) \big[A_E(\arg(\mathbf{r}' - \mathbf{r}) - \phi_s(\mathbf{r})) P_O(\phi_s(\mathbf{r}) - \phi_s(\mathbf{r}')) - A_O(\arg(\mathbf{r}' - \mathbf{r}) - \phi_s(\mathbf{r})) P_E(\phi_s(\mathbf{r}) - \phi_s(\mathbf{r}')) \big] d\mathbf{r}'. \tag{4.8}$$

It is straightforward to establish the existence of the synchronous solution $\phi_s(\mathbf{r}) = \phi_0$. That is, the first term in the integral then trivially vanishes since $P_O(0) = 0$, whereas the second term in the integral becomes

$$\begin{aligned}
&\int_{\mathbb{R}^2} w_s(|\mathbf{r}-\mathbf{r}'|)A_O(\arg(\mathbf{r}'-\mathbf{r})-\phi_s(\mathbf{r}))P_E(\phi_s(\mathbf{r})-\phi_s(\mathbf{r}'))d\mathbf{r}' \\
&= P_E(0)\int_{\mathbb{R}^2} w_s(|\mathbf{r}-\mathbf{r}'|)A_O(\arg(\mathbf{r}'-\mathbf{r})-\phi_0)d\mathbf{r}' \\
&= P_E(0)\int_0^\infty \rho' w_s(\rho')\int_0^{2\pi} A_O(\theta'-\phi_0)d\theta' d\rho' = 0
\end{aligned}$$

since A_O is odd and π-periodic.

Proceeding along similar lines to the isotropic case, we set $\phi(\mathbf{r},\tau) = \phi_0 + \varepsilon\psi(\mathbf{r})e^{\lambda\tau}$ and Taylor expand each term in (3.9) to first order in ε. This yields the eigenvalue problem

$$\lambda\psi(\mathbf{r}) = -P_O'(0)\int_{\mathbb{R}^2} w_s(|\mathbf{r}-\mathbf{r}'|)A_E(\arg(\mathbf{r}'-\mathbf{r})-\phi_0)[\psi(\mathbf{r})-\psi(\mathbf{r}')]d\mathbf{r}.' \tag{4.9}$$

We have used the fact that $P_E'(0) = 0$, $P_O(0) = 0$, and

$$\int_{\mathbb{R}^2} w_s(|\mathbf{r}'|)A_O'(\arg(\mathbf{r}')-\phi_0)d\mathbf{r}' = \int_0^\infty \rho w_s(\rho)d\rho\int_0^{2\pi} A_O'(\theta-\phi_0)d\theta = 0$$

since A_O is continuous and π-periodic. Again the eigenfunctions are given by (4.2). Substituting into the eigenvalue equation, introducing polar coordinates, and using

$$\int_{\mathbb{R}^2} w_s(|\mathbf{r}'|)A_E(\arg(\mathbf{r}')-\phi_0)d\mathbf{r}' = \int_0^{2\pi} A_E(\theta-\phi_0)d\theta\int_0^\infty \rho w_s(\rho)d\rho \equiv 2A_{E,0}w_{s,0},$$

we have

$$\lambda(q,\theta_q) = -P_O'(0)\left(2w_{s,0}A_{E,0} - \int_0^\infty\int_0^{2\pi}\rho' w_s(\rho')A_E(\theta')e^{iq\rho'\cos(\theta+\phi_0-\theta_q)}d\theta' d\rho'\right).$$

The Jacobi–Anger expansion (4.4) then yields

$$\begin{aligned}
\lambda(q,\theta_q) = &-2P_O'(0)A_{E,0}\left[w_{s,0} - \int_0^\infty \rho w_s(\rho)J_0(\rho q)d\rho\right] \\
&+ 2P_O'(0)\sum_{n=1}^\infty i^n\int_0^\infty \rho w_s(\rho)J_n(\rho q)d\rho\int_0^{2\pi} A_E(\theta)\cos(n(\theta+\phi_0-\theta_q))d\theta.
\end{aligned}$$

Introducing the Fourier series for the π-periodic function

$$A(\theta) = \frac{1}{\pi}\left[A_0 + 2\sum_{m=0}^\infty A_{2m}\cos(2m\theta)\right]$$

and using the trigonometric identity

$$\cos(n(\theta+\phi_0-\theta_q)) = \cos(n\theta)\cos(n(\phi_0-\theta_q)) - \sin(n\theta)\sin(n(\phi_0-\theta_q))$$

we find that

$$\int_0^{2\pi} A_E(\theta)\cos\left(n(\theta+\phi_0-\theta_q)\right)d\theta = \frac{\cos(n\Delta)}{|V_0'(\Delta)|}A_n\cos\left(n(\phi_0-\theta_q)\right)\delta_{n,2m}$$

for any nonzero integer integer m. Finally, noting that

$$\int_0^{\infty}\rho w_s(\rho)J_n(q\rho)d\rho = \mathcal{H}_n[w_s](q),$$

the eigenvalues reduce to

$$\lambda(q,\theta_q) = \underbrace{A_0(\mathcal{H}_0[w_s](q)-\mathcal{H}_0[w_s](0))}_{\text{isotropic part}} + 2\sum_{n=1}^{\infty}\underbrace{(-1)^n A_{2n}\cos(2n\Delta)\mathcal{H}_{2n}[w_s](q)\cos\left(2n(\phi_0-\theta_q)\right)}_{\text{anisotropic part}}, \tag{4.10}$$

where, for notational clarity, we have neglected $P_O'(0)/|V_0'(\Delta)|$ since $P_O'(0) > 0$ and the magnitude does not contribute to stability. Note that convergence of the series follows from the fact

$$|\mathcal{H}_{2n}[w_s](q)| \le \mathcal{H}_0[w_s](0)$$

for all $n \ge 0$, and assuming that A has a convergent Fourier series, hence so does A_E, easily shows absolute convergence. Since $\mathcal{H}_{2n}[w_s](0) = 0$ for $n \ge 1$, we have that $\lambda = 0$ when $q = 0$ corresponding to the shift-twist invariance of the system. For isotropic connections the eigenvalues are simply

$$\lambda(q,\theta_q) = A_0(\mathcal{H}_0[w_s](q)-\mathcal{H}_0[w_s](0)).$$

If w_s is positive (excitatory) and monotonically decreasing sufficiently fast, we have that $\mathcal{H}_0[w_s](q) > 0$ for all $q > 0$. An example of a function is the Gaussian,

$$\mathcal{H}_0\left[e^{-(x^2+y^2)/2\sigma^2}\right] = \sigma^2 e^{-q^2\sigma^2/2}.$$

Therefore, since $|\mathcal{H}_0[w_s](q)| < \mathcal{H}_0[w_s](0)$ we have that $\lambda(q,\theta_q) < 0$ for all $q > 0$ and $\theta_q \in [0, 2\pi)$. Hence, in the case of isotropic connections and excitatory w_s, the synchronous solution is stable.

An interesting question is whether the synchronous state can be destabilized by anisotropic connections. Here we show that stability persists in the presence of anisotropy of the particular form $A(\theta) = [1+\cos(2\theta)]/\pi$. This is chosen for mathematical convenience but can be interpreted as an example of relatively weak anisotropy. Furthermore, we take w_s to be a Gaussian; see (4.6). The eigenvalues are then given by

$$\lambda(q,\Delta\theta) = \mathcal{H}_0[w_s](q) - \mathcal{H}_0[w_s](0) - \mathcal{H}_2[w_s](q)\cos(2\Delta)\cos(2\Delta\theta), \quad \Delta\theta = \phi_0-\theta_q.$$

In the case of a Gaussian for w_s, we have that $\mathcal{H}_2[w_s](q) > 0$ and therefore an upper bound for λ is given by

$$\lambda^+(q) \equiv \mathcal{H}_0[w_s](q) - \mathcal{H}_0[w_s](0) + \mathcal{H}_2[w_s](q) \ge \lambda(q,\Delta\theta).$$

We can explicitly compute the Hankel transforms for the Gaussian as

$$\mathcal{H}_0[w_s](q) = \frac{1}{2\pi} e^{-q^2\sigma^2/2}, \quad \mathcal{H}_2[w_s](q) = \frac{2 - e^{-q^2\sigma^2/2}(2+\sigma^2 q^2)}{2\pi q^2 \sigma^2},$$

and we obtain

$$\lambda^+(q) = \frac{2 - 2e^{-q^2\sigma^2/2} - \sigma^2 q^2}{2\pi\sigma^2 q^2}.$$

which is easy to show is negative for all $q > 0$. Hence, the synchronous solution is stable in the presence of the given form of anisotropy.

4.4. Angular solution. In all the examples so far we have taken the active region to be $U = \mathbb{R}^2$. As our final example we establish the existence of the angular solution

$$\phi_s(\mathbf{r}) = \begin{cases} \arg(\mathbf{r}), & \mathbf{r} \neq 0, \\ 0, & \mathbf{r} = 0, \end{cases}$$

on any annular domain $U = \{R_1 \leq |\mathbf{r}| \leq R_2\}$. Note that there is no way to define this continuously at $\mathbf{r} = 0$, so we therefore define $\phi_s(0) = 0$ for convenience; however, this choice is arbitrary. Let $\Gamma(\mathbf{r})$ denote the right-hand side of (4.8). First note that $\arg(\kappa_x \mathbf{r}) = -\arg(\mathbf{r})$ for all $\mathbf{r} \neq 0$, where κ_x is the reflection, $(x, y) \mapsto (-x, y)$. We then have that $\Gamma(\kappa_x \mathbf{r}) = -\Gamma(\mathbf{r})$ for all $\mathbf{r} \in \mathbb{R}^2$ since

$$\begin{aligned}
&\int_U w_s(|\kappa_x \mathbf{r} - \mathbf{r}'|) A_E(\arg(\mathbf{r}' - \kappa_x \mathbf{r}) - \arg(\kappa_x \mathbf{r})) P_O(\arg(\kappa_x \mathbf{r}) - \arg(\mathbf{r}')) \\
&= \int_{\kappa_x U} w_s(|\kappa_x(\mathbf{r} - \mathbf{r}')|) A_E(\arg(\kappa_x(\mathbf{r}' - \mathbf{r})) + \arg(\mathbf{r})) P_O(-\arg(\mathbf{r}) - \arg(\kappa_x \mathbf{r}')) d\mathbf{r}' \\
&= \int_U w_s(|\mathbf{r} - \mathbf{r}'|) A_E(-\arg(\mathbf{r}' - \mathbf{r}) + \arg(\mathbf{r})) P_O(-\arg(\mathbf{r}) + \arg(\mathbf{r}')) d\mathbf{r}' \\
&= -\int_U w_s(|\mathbf{r} - \mathbf{r}'|) A_E(\arg(\mathbf{r}' - \mathbf{r}) - \arg(\mathbf{r})) P_O(\arg(\mathbf{r}) - \arg(\mathbf{r}')) d\mathbf{r}',
\end{aligned}$$

where we have used the fact that $\kappa_x U = U$ and the change in sign is due to the fact that P_O is odd while A_E is even. Similarly

$$\begin{aligned}
&\int_U w_s(|\kappa_x \mathbf{r} - \mathbf{r}'|) A_O(\arg(\mathbf{r}' - \kappa_x \mathbf{r}) - \arg(\kappa_x \mathbf{r})) P_E(\arg(\kappa_x \mathbf{r}) - \arg(\mathbf{r}')) d\mathbf{r}' \\
&= -\int_U w_s(|\mathbf{r} - \mathbf{r}'|) A_O(\arg(\mathbf{r}' - \mathbf{r}) - \arg(\mathbf{r})) P_E(\arg(\mathbf{r}) - \arg(\mathbf{r}')) d\mathbf{r}'
\end{aligned}$$

since A_O is odd and P_E is even. On the other hand, since $\arg(\mathcal{R}_\theta \mathbf{r}) = \arg(\mathbf{r}) + \theta$ and $\mathcal{R}_\theta U = U$ we have that $\Gamma(\mathcal{R}_\theta \mathbf{r}) = \Gamma(\mathbf{r})$ for any $\theta \in [0, 2\pi)$ and $\mathbf{r} \in \mathbb{R}^2$. However, for $\theta = -2 \arg \mathbf{r}$ we have that $\Gamma(\mathbf{r}) = \Gamma(\mathcal{R}_{-2\arg \mathbf{r}} \mathbf{r}) = \Gamma(\kappa_x \mathbf{r}) = -\Gamma(\mathbf{r})$ since reflection is the same as clockwise rotation by twice the angle. Thus it must be true that $\Gamma(\mathbf{r}) = 0$ for all $\mathbf{r}$ and hence $\phi_s(\mathbf{r}) = \arg(\mathbf{r})$ is a solution. It also follows that $\phi_s(\mathbf{r}) = \arg(\mathbf{r}) \pm \pi/2$ is a solution since

$$A_i\left(\theta + \frac{\pi}{2}\right) = A_i\left(\theta - \frac{\pi}{2}\right), \quad i = E, O.$$

5. Numerical simulations of full neural field equation. We now present results from numerical simulations of the full neural field equation in (1.4) in order to show consistency with the analysis of the phase equation. Note we are assuming that in the absence of horizontal connections bump solutions are stable. We therefore expect that any instabilities that occur in the full neural field equations are due to the long-range connections. Furthermore, since the long-range connections are weak, we don't expect them to cause any instabilities in the amplitude of the bumps but rather in the phase of the bumps. It is then reasonable to assume that stability results for the phase equation obtained in section 5 will translate to stability for the full system when restricting to phase changing perturbations.

The numerical methods we use are as follows. Integration in time is computed using Euler's method with step sizes $\Delta t = 0.01$. We discretize space and orientation on a $300 \times 300 \times 200$ grid. The spatially independent convolution integral in (1.4) is computed using a trapezoidal rule. The space-orientation integral is computed by first using a trapezoidal rule to integrate along the orientation direction at each point in space, and then the remaining spatial convolution is computed using fast Fourier transforms. We take initial conditions $v(\mathbf{r}, \theta, 0) = V_0(\theta - \phi(\mathbf{r}) - \psi(\mathbf{r}))$, where V_0 is defined in section 3, $\phi(\mathbf{r})$ is a stationary phase solution described in section 5, and $\psi(\mathbf{r})$ is the perturbation. Recall that our stability analysis of solutions to the phase equation implicitly considers perturbations in the phase of the bump, and we therefore only consider phase changing perturbations in our numerical simulations. We compute V_0 by numerically solving the threshold equation, $\kappa - \gamma = W(2\Delta)$ for the bump width Δ. To generate the figures we numerically simulate the full neural field equations to obtain a solution $v(\mathbf{r}, \theta, t)$, and at each time step and point in space we find the orientation at which v is a maximum, indicating the orientation of the bump peak. Defining $\varphi(\mathbf{r}, t)$ such that

$$v(\mathbf{r}, \varphi(\mathbf{r}, t), t) = \max_{\theta \in [0, 2\pi)} v(\mathbf{r}, \theta, t)$$

we give a density plot for $\varphi(\mathbf{r}, t)$ and superimpose this with a vector field

$$x(\mathbf{r}, t) = \cos \varphi(\mathbf{r}, t), \quad y(\mathbf{r}, t) = \sin \varphi(\mathbf{r}, t)$$

to illustrate the fact that $\varphi(\mathbf{r}, t)$ indicates the orientation of local contours at point $\mathbf{r}$ and time t.

In Figures 5–7 we show simulations of the linear phase solution $\phi_s(\mathbf{r}) = \mathbf{k} \cdot \mathbf{r} + \phi_0$. We first let $\mathbf{k} = (1, 1)$, which, according to our stability analysis, is most unstable to perturbations along $\mathbf{k}$, $\mathbf{q} = \alpha \mathbf{k}$. Since we set $\sigma = 0.5$, then we have that $|\mathbf{k}| > 1/2\sigma$, and therefore our analysis predicts that the linear phase solution will be unstable. In Figure 5(a) we perturb the linear phase solution with $\mathbf{q} = 2\mathbf{k}$ and see that the solution destabilizes and settles at approximately the synchronous solution, verifying the stability analysis. In Figure 5(b) we perturb the solution with $\mathbf{q} = 2\mathbf{k}^{\perp}$ and see that the solution tends back toward the linear phase solution, indicating stability with respect to orthogonally directed perturbations as predicted by our analysis. Next, in Figure 6(a)–(b) we perturb the solution with $\mathbf{q} = 10\mathbf{k}$ and $\mathbf{q} = 10\mathbf{k}^{\perp}$. We see that, in both cases, the solution tends back toward the linear phase solution, again in agreement with our stability analysis. Finally we set $\mathbf{k} = (1/2, 1/2)$ so that $|\mathbf{k}| < 1/2\sigma$ and we are in a regime where the linear phase solution is stable to perturbations in all directions and magnitudes. In Figure 7(a)–(b) we show perturbations with $\mathbf{q} = 2\mathbf{k}$ and $\mathbf{q} = 2\mathbf{k}^{\perp}$ and

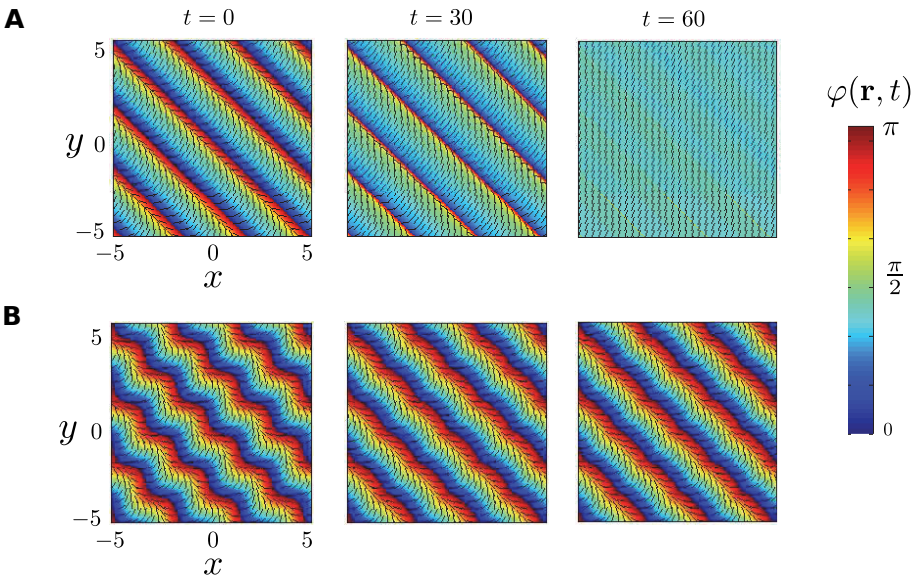

Figure 5. *Numerical simulation of the linear phase solutions using the original neural field equation. Initial conditions are given by (2.6) with $\phi(\mathbf{r}) = \mathbf{k}\cdot\mathbf{r} + \psi(\mathbf{r})$, where $\psi(\mathbf{r})$ is the perturbation. Here we take $\mathbf{k} = (1, 1)$. (a) Perturbation in the direction of linear phase solution, $\mathbf{q} = 2\mathbf{k}$. (b) Perturbation in the orthogonal direction, $\mathbf{q} = 2\mathbf{k}^{\perp}$. Parameter values are given by $\varepsilon = 0.3$, $\sigma = 0.5$, $(w_{\rm hoz})_0 = \pi$, $\kappa = 2$, $\gamma = 2.5$, $(w_{\rm hoz})_2 = \pi/2$.*

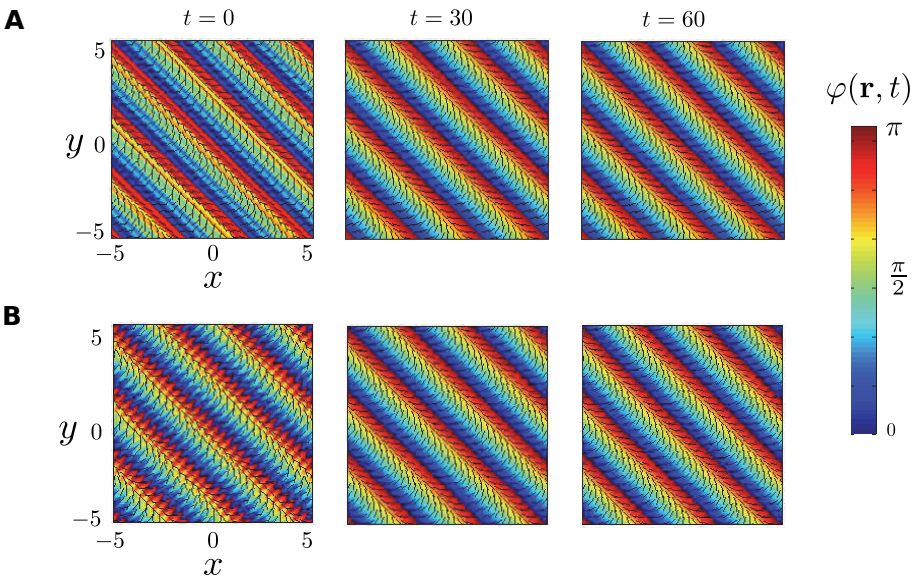

Figure 6. *Numerical simulation of the linear phase solutions using the original neural field equation. Initial conditions are given by (2.6) with $\phi(\mathbf{r}) = \mathbf{k}\cdot\mathbf{r} + \psi(\mathbf{r})$, where $\psi(\mathbf{r})$ is the perturbation. Here we take $\mathbf{k} = (1, 1)$. (a) Perturbation in the direction of linear phase solution, $\mathbf{q} = 10\mathbf{k}$. (b) Perturbation in the orthogonal direction, $\mathbf{q} = 10\mathbf{k}^{\perp}$. Parameter values are given by $\varepsilon = 0.3$, $\sigma = .05$, $\kappa = 2$, $\gamma = 2.5$, $(w_{\rm hoz})_0 = \pi$, $(w_{\rm hoz})_2 = \pi/2$.*

we see that the solution is now stable to perturbations that destabilized the solution in the previous case.

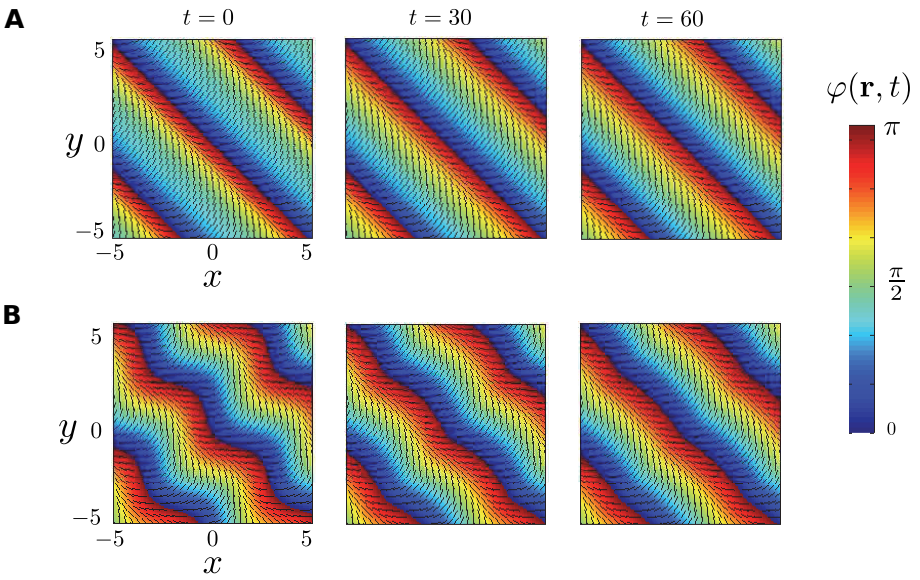

Figure 7. *Numerical simulation of the linear phase solutions using the original neural field equation. Initial conditions are given by (2.6) with $\phi(\mathbf{r}) = \mathbf{k} \cdot \mathbf{r} + \psi(\mathbf{r})$, where $\psi(\mathbf{r})$ is the perturbation. Here we take $\mathbf{k} = (1/2, 1/2)$. (a) Perturbation in the direction of linear phase solution, $\mathbf{q} = 2\mathbf{k}$. (b) Perturbation in the orthogonal direction, $\mathbf{q} = 2\mathbf{k}^{\perp}$. Parameter values are given by $\varepsilon = 0.3$, $\sigma = 0.5$, $\kappa = 2$, $\gamma = 2.5$, $(w_{\text{hoz}})_0 = \pi$, $(w_{\text{hoz}})_2 = \pi/2$.*

Finally we simulate the angular phase solutions,

$$\phi_s(\mathbf{r}) = \arg(\mathbf{r}) \quad \text{and} \quad \phi_s(\mathbf{r}) = \arg(\mathbf{r}) + \frac{\pi}{2},$$

in the region $U = \{\mathbf{r} \in \mathbb{R}^2 | 2 \leq |\mathbf{r}| \leq 4\}$. Since we have not provided a stability analysis for this solution we arbitrarily add random noise to the initial condition to check, numerically, that the angular phase is a solution to the original neural field equation. In Figure 8 we show a simulation for both of these solutions and see that the solution indeed does tend toward the angular phase described above.

6. Discussion. In this paper we explored the affects of excitatory, long-range horizontal connections on spatially organized patterns of orientation selectivity in the strongly nonlinear regime using the constructive approach of Amari [1]. In particular, we derived a phase equation that determines the spatiotemporal dynamics of the phase of orientation tuning curves. In essence, the phase equation reduces the dimension of the full neural field equation when considering a certain class of solutions. The main benefit of this reduced equation is that it is much simpler in form than the original neural field equation and allows us to show the existence of some complex solutions with relatively little effort. Showing existence of these solutions in the original neural field equation would be a very arduous, if not impossible, task. Moreover, we expect that the simplicity of the phase equation will lead to greater analytical insights to visual perceptual phenomenon in general.

One obvious extension of our analysis is to include orientation-dependent inputs. Here we briefly point out one interesting observation. Suppose that $\phi_s(\mathbf{r})$ is some natural stationary

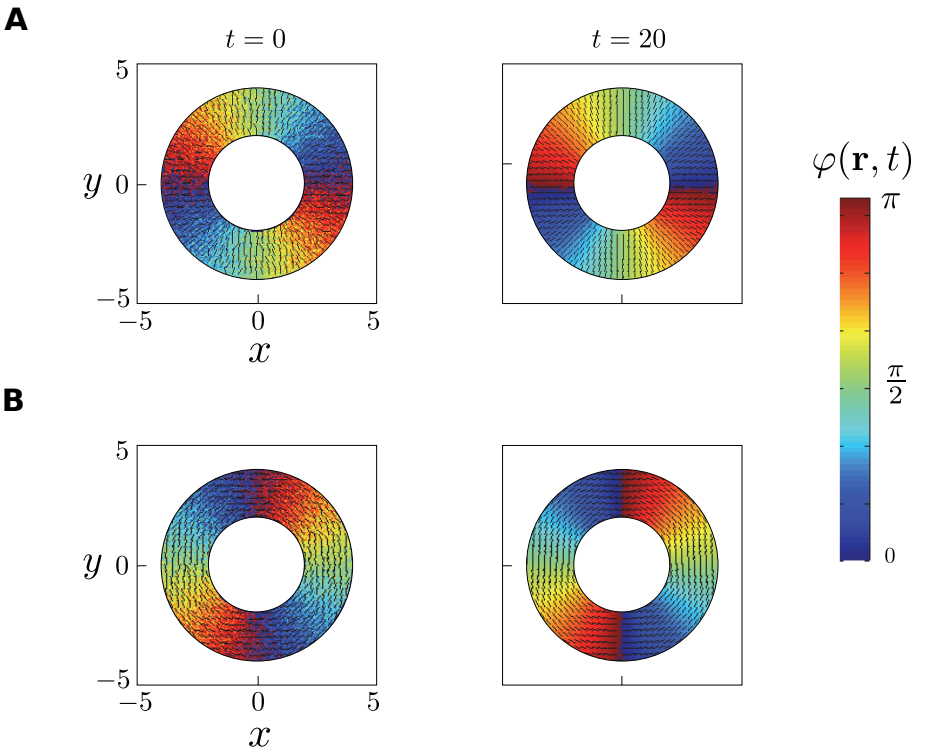

Figure 8. *Numerical simulation of the angular phase solutions using the original neural field equation. Initial conditions are given by (2.6) with $\phi(\mathbf{r}) = \mathbf{k}\cdot\mathbf{r}+\psi(\mathbf{r})$, where $\psi(\mathbf{r})$ is the perturbation. (A) Radial angular solution $\phi(\mathbf{r}) = \arg(\mathbf{r})$ plus random noise. (B) Tangential angular solution $\phi(\mathbf{r}) = \arg(\mathbf{r}) + \pi/2$ plus random noise. Parameter values are given by $\varepsilon = .3$, $\sigma = .5$, $\kappa = 2$, $\gamma = 2.5$, $(w_{\rm hoz})_0 = A_0 = \pi$, $(w_{\rm hoz})_2 = A_2 = \pi/2$.*

solution to (3.9) with $I_O = 0$. If the orientation of the external input is given exactly by the stationary solution, $\theta_0(\mathbf{r}) = \phi_s(\mathbf{r})$, then we have that $I_O(\phi_s(\mathbf{r}) - \theta_0(\mathbf{r})) = I_O(0) = 0$. Hence $\phi_s(\mathbf{r})$ is also a stationary solution to the phase equation with nonzero input. Furthermore, perturbing the stationary solution, $\phi(\mathbf{r},\tau) = \theta_0(\mathbf{r}) + \varepsilon\psi(\mathbf{r})e^{\lambda\tau}$, and linearizing I_O yields

$$I_O(\phi(\mathbf{r},\tau) - \theta_0(\mathbf{r})) = I_O(0) + \varepsilon I_O'(0)\psi(\mathbf{r})e^{\lambda\tau} = -\frac{\varepsilon I_1'(\Delta)}{|V_0'(\Delta)|}\psi(\mathbf{r})e^{\lambda\tau}.$$

Hence if λ_0 is an eigenvalue with respect to solutions without input, then

$$\lambda_I = \frac{I_1'(\Delta)}{|V_0'(\Delta)|} + \lambda_0$$

is an eigenvalue with respect to solutions with input. In particular, if I_1 is a monotonically decreasing function, then $I_1'(\Delta) \le 0$, in which case the presence of an input at most only decreases the eigenvalues and therefore can only make the solutions more stable. In general, if I_1 is not monotonically decreasing, then the bump width Δ may have an affect on the stability of stationary solutions. In future work, we hope to explore in more detail existence and stability of stationary solutions when $\theta_0(\mathbf{r})$ is not a natural stationary solution.

The inclusion of orientation-dependent inputs would then allow us to use the phase equation to study various visual processing phenomena such as contextual effects, perceptual completion, and perceptual grouping, to name a few. Perceptual completion and grouping have been studied using geometric approaches in [33] and a combination of geometry and neural fields in [18]. Specifically, in [33] the authors show that perceptual grouping can be understood by looking at the dominant eigenmodes of the corresponding affinity matrix. That is, if the network is presented with a stimulus which contains both randomly oriented line segments and a coherent perceptual unit, the dominant eigenmodes isolate the coherent part of the stimulus from the noisy part. One can construct a similar setup using the phase equation where U is now a collection of disjoint sets, determined by the segmented input, and study how the phase correlates among the different regions. The phase along a coherent perceptual unit should be more highly correlated than the phase along randomly oriented regions. Applying our analysis to contextual effects will also require allowing for inhibitory long-range connections. For although such connections are mediated by axonal projections from excitatory pyramidal neurons, these projections innervate both pyramidal cells and feedforward inhibitory neurons. Hence, physiologically speaking, horizontal connections can be excitatory or inhibitory, depending on stimulus conditions [2].

Another application of our analysis is to revisit the theory of geometric visual hallucinations along the lines of [15] and to see if there are analogous results within the context of the phase equation in the strongly nonlinear regime. In order to generate hallucinatory patterns in the coupled ring model (1.4), Bressloff et al. [15] assumed that the spatial distribution of horizontal connections consisted of short-range excitation and long-range inhibition, that is, the weight function w_s was taken to be a Mexican hat function. However, it is more likely that such a structure occurs at the local level within a single hypercolumn, that is, within $\mathbb{S}^1$. Therefore, we also aim to extend the coupled ring model to take into account the laminar structure of V1, with the idea that a local Mexican hat function in an orientation-independent deep cortical layer generates a spatially periodic pattern via a Turing-like instability, which then provides a spatially structured input to an orientation-dependent superficial layer described by the coupled ring model (1.4). We have recently constructed such a model to study propagating waves of orientation selectivity in V1 [12].

REFERENCES

[1] S. Amari, *Dynamics of pattern formation in lateral inhibition type neural fields*, Biol. Cybern et., 27 (1977), pp. 77–87.

[2] A. Angelucci, J. B. Levitt, E. J. S. Walton, J.-M. Hupe, J. Bullier, and J. S. Lund, *Circuits for local and global signal integration in primary visual cortex*, J. Neurosci., 22 (2002), pp. 8633–8646.

[3] O. Ben-Shahar and S. W. Zucker, *Geometrical computations explain projection patterns of long range horizontal connections in visual cortex*, Neural Comput., 16 (2004), pp. 445–476.

[4] R. Ben-Yishai, R. Lev Bar-Or, and H. Sompolinsky, *Theory of orientation tuning in visual cortex*, Proc. Natl. Acad. Sci. USA, 92 (1995), pp. 3844–3848.

[5] G. G. Blasdel, *Orientation selectivity, preference, and continuity in monkey striate cortex*, J. Neurosci., 12 (1992), pp. 3139–3161.

[6] G. G. Blasdel and G. Salama, *Voltage-sensitive dyes reveal a modular organization in monkey striate cortex*, Nature, 321 (1986), pp. 579–585.

[7] T. Bonhoeffer and A. Grinvald, *Orientation columns in cat are organized in pinwheel like patterns*, Nature, 364 (1991), pp. 166–146.
[8] W. H. Bosking, Y. Zhang, B. Schofield, and D. Fitzpatrick, *Orientation selectivity and the arrangement of horizontal connections in tree shrew striate cortex*, J. Neurosci., 17 (1997), pp. 2112–2127.
[9] P. C. Bressloff, *Spatially periodic modulation of cortical patterns by long-range horizontal connections*, Phys. D, 185 (2003), pp. 131–157.
[10] P. C. Bressloff, *Spatiotemporal dynamics of continuum neural fields: Invited topical review*, J. Phys. A, 45 (2012), 033001.
[11] P. C. Bressloff and S. R. Carroll., *Spatio-temporal dynamics of neural fields on product spaces*, SIAM J. Appl. Dyn. Syst., 13 (2014), pp. 1620–1653.
[12] P. C. Bressloff and S. R. Carroll, *Laminar neural field model of laterally propagating waves of orientation selectivity*, PLoS Comput. Biol., 11 (2015), e1004545.
[13] P. C. Bressloff and J. D. Cowan, *Amplitude equation approach to contextual effects in visual cortex*, Neural Comput., 14 (2002), pp. 493–525.
[14] P. C. Bressloff, J. D. Cowan, M. Golubitsky, and P. J. Thomas, *Scalar and pseudoscalar bifurcations: Pattern formation on the visual cortex*, Nonlinearity, 14 (2001), pp. 739–775.
[15] P. C. Bressloff, J. D. Cowan, M. Golubitsky, P. J. Thomas, and M. Wiener, *Geometric visual hallucinations, euclidean symmetry and the functional architecture of striate cortex*, Philos. Trans. Roy. Soc. Lond. Ser. B, 356 (2001), pp. 299–330.
[16] S. R. Carroll and P. C. Bressloff, *Binocular rivalry waves in directionally selective neural field models*, Phys. D, 285 (2014), pp. 8–17.
[17] P. Chossat, G. Faye, and O. Faugeras, *Bifurcation of hyperbolic planforms*, J Nonlinear Sci. 21 (2011), pp. 465–498.
[18] G. Citti and A. Sarti, *A cortical based model of perceptual completion in the roto-translation space*, J. Math. Imaging Vision, 24 (2006), pp. 307–326.
[19] G. B. Ermentrout, *Neural networks as spatio-temporal pattern-forming systems*, Rep. Progr. Phys., 61 (1998), pp. 353–430.
[20] G. B. Ermentrout and J. Cowan, *A mathematical theory of visual hallucination patterns*, Biol. Cybern et., 34 (1979), pp. 137–150.
[21] G. B. Ermentrout and D. Kleinfeld, *Traveling electrical waves in cortex: Insights from phase dynamics and speculation on a computational role*, Neuron, 29 (2001), pp. 33–44.
[22] C. D. Gilbert, *Horizontal integration and cortical dynamics*, Neuron, 9 (1992), pp. 1–13.
[23] C. D. Gilbert, A. Das, M. Ito, M. Kapadia, and G. Westheimer, *Spatial integration and cortical dynamics.*, Proc. Natl. Acad. Sci. USA, 93 (1996), pp. 615–622.
[24] C. D. Gilbert and T. N. Wiesel, *Clustered intrinsic connections in cat visual cortex*, J. Neurosci., 3 (1983), pp. 1116–1133.
[25] S. Heitmann, P. Gong, and M. Breakspear, *A computational role for bistability and traveling waves in motor cortex*, Front. Comput. Neurosci., 6 (2012), pp. 1–15.
[26] J. D. Hirsch and C. D. Gilbert, *Synaptic physiology of horizontal connections in the cat's visual cortex*, J. Physiol. Lond., 160 (1991), pp. 106–154.
[27] D. H. Hubel and T. N. Wiesel, *Sequence regularity and geometry of orientation columns in the monkey striate cortex*, J. Comput. Neurol., 158 (1974), pp. 267–294.
[28] D. H. Hubel and T. N. Wiesel, *Uniformity of monkey striate cortex: A parallel relationship between field size, scatter, and magnification factor*, J. Comput. Neurol., 158 (1974), pp. 295–306.
[29] S. LeVay and S. B. Nelson, *Columnar organization of the visual cortex*, in The Neural Basis of Visual Function, A. G. Leventhal, ed., CRC Press, Boca Raton, FL, 1991, pp. 266–315.
[30] R. Malach, Y. Amirand, M. Harel, and A. Grinvald, *Relationship between intrinsic connections and functional architecture revealed by optical imaging and in vivo targeted biocytin injections in primate striate cortex*, Proc. Natl. Acad. Sci. USA, 90 (1993), pp. 0469–10473.
[31] J. Petitot, *The neurogeometry of pinwheels as a sub-Riemannian contact structure*, J. Physiol. Paris, 97 (2003), pp. 265–309.
[32] K. S. Rockland and J. Lund, *Intrinsic laminar lattice connections in primate visual cortex*, J. Comput. Neurol., 216 (1983), pp. 303–318.

[33] A. Sarti and G. Citti, *The constitution of visual perceptual units in the function architecture of v*1, J. Comp. Neurosci., 38 (2014), pp. 285–300.
[34] A. Sarti, G. Citti, and J. Petitot, *The symplectic structure of the primary visual cortex*, Biol. Cybern et., (2008), pp. 33–48.
[35] L. Schwabe, K. Obermayer, A. Angelucci, and P. C. Bressloff, *The role of feedback in shaping the extra-classical receptive field of cortical neurons: A recurrent network model*, J. Neurosci., 26 (2006), pp. 9117–9129.
[36] L. C. Sincich and G. G. Blasdel, *Oriented axon projections in primary visual cortex of the monkey*, J. Neurosci., 21 (2001), pp. 4416–4426.
[37] D. C. Somers, S. Nelson, and M. Sur, *An emergent model of orientation selectivity in cat visual cortical simple cells*, J. Neurosci., 15 (1995), pp. 5448–5465.
[38] N. V. Swindale, *The development of topography in the visual cortex: A review of models*, Network, 7 (1996), pp. 161–274.
[39] D. A. Wiley, S. H. Strogatz, and M. Girvan, *The size of the sync basin*, Chaos, 16 (2006), 015103.
[40] X. Xie and M. Giese, *Nonlinear dynamics of direction-selective recurrent neural media*, Phys. Rev. E, 65 (2002), 051904.
[41] T. Yoshioka, G. G. Blasdel, J. B. Levitt, and J. S. Lund, *Relation between patterns of intrinsic lateral connectivity, ocular dominance, and cytochrome oxidase–reactive regions in macaque monkey striate cortex*, Cerebral Cortex, 6 (1996), pp. 297–310.